AMERICAN SOCIETY FOR MICROBIOLOGY | Journal of Virology®

ϕX174 Procapsid Assembly: Effects of an Inhibitory External Scaffolding Protein and Resistant Coat Proteins *In Vitro*

James E. Cherwa, Jr.,[a] Joshua Tyson,[a] Gregory J. Bedwell,[b] Dewey Brooke,[b] Ashton G. Edwards,[c] Terje Dokland,[b] Peter E. Prevelige,[b] Bentley A. Fane[d]

Department of Biology, Central Alabama Community College, Alexander City, Alabama, USA[a]; Department of Microbiology, University of Alabama at Birmingham, Birmingham, Alabama, USA[b]; Jefferson County International Baccalaureate School, Birmingham, Alabama, USA[c]; School of Plant Sciences and the BIO5 Institute, University of Arizona, Tucson, Arizona, USA[d]

ABSTRACT During ϕX174 morphogenesis, 240 copies of the external scaffolding protein D organize 12 pentameric assembly intermediates into procapsids, a reaction reconstituted *in vitro*. In previous studies, ϕX174 strains resistant to exogenously expressed dominant lethal D genes were experimentally evolved. Resistance was achieved by the stepwise acquisition of coat protein mutations. Once resistance was established, a stimulatory D protein mutation that greatly increased strain fitness arose. In this study, *in vitro* biophysical and biochemical methods were utilized to elucidate the mechanistic details and evolutionary trade-offs created by the resistance mutations. The kinetics of procapsid formation was analyzed *in vitro* using wild-type, inhibitory, and experimentally evolved coat and scaffolding proteins. Our data suggest that viral fitness is correlated with *in vitro* assembly kinetics and demonstrate that *in vivo* experimental evolution can be analyzed within an *in vitro* biophysical context.

IMPORTANCE Experimental evolution is an extremely valuable tool. Comparisons between ancestral and evolved genotypes suggest hypotheses regarding adaptive mechanisms. However, it is not always possible to rigorously test these hypotheses *in vivo*. We applied *in vitro* biophysical and biochemical methods to elucidate the mechanistic details that allowed an experimentally evolved virus to become resistant to an antiviral protein and then evolve a productive use for that protein. Moreover, our results indicate that the respective roles of scaffolding and coat proteins may have been redistributed during the evolution of a two-scaffolding-protein system. In one-scaffolding-protein virus assembly systems, coat proteins promiscuously interact to form heterogeneous aberrant structures in the absence of scaffolding proteins. Thus, the scaffolding protein controls fidelity. During ϕX174 assembly, the external scaffolding protein acts like a coat protein, self-associating into large aberrant spherical structures in the absence of coat protein, whereas the coat protein appears to control fidelity.

KEYWORDS bacteriophage ϕX174, *Microviridae*, microvirus, scaffolding protein, virus assembly

Received 16 September 2016 **Accepted** 18 October 2016

Accepted manuscript posted online 26 October 2016

Citation Cherwa JE, Jr., Tyson J, Bedwell GJ, Brooke D, Edwards AG, Dokland T, Prevelige PE, Fane BA. 2017. ϕX174 procapsid assembly: effects of an inhibitory external scaffolding protein and resistant coat proteins *in vitro*. J Virol 91:e01878-16. https://doi.org/10.1128/JVI.01878-16.

Editor Rozanne M. Sandri-Goldin, University of California, Irvine

Copyright © 2016 American Society for Microbiology. All Rights Reserved.

Address correspondence to James E. Cherwa, Jr., jcherwajr@cacc.edu.

Due to their rapid replication cycle, detailed structural information, and well developed genetic and biochemical assays, the microviruses have become an ideal model system for experimental evolution (1–4). The morphogenetic pathway can be characterized under restrictive conditions and adaptive mutations can be mapped onto X-ray structures, providing insights into evolutionary mechanisms and protein structure-function relationships (2–8).

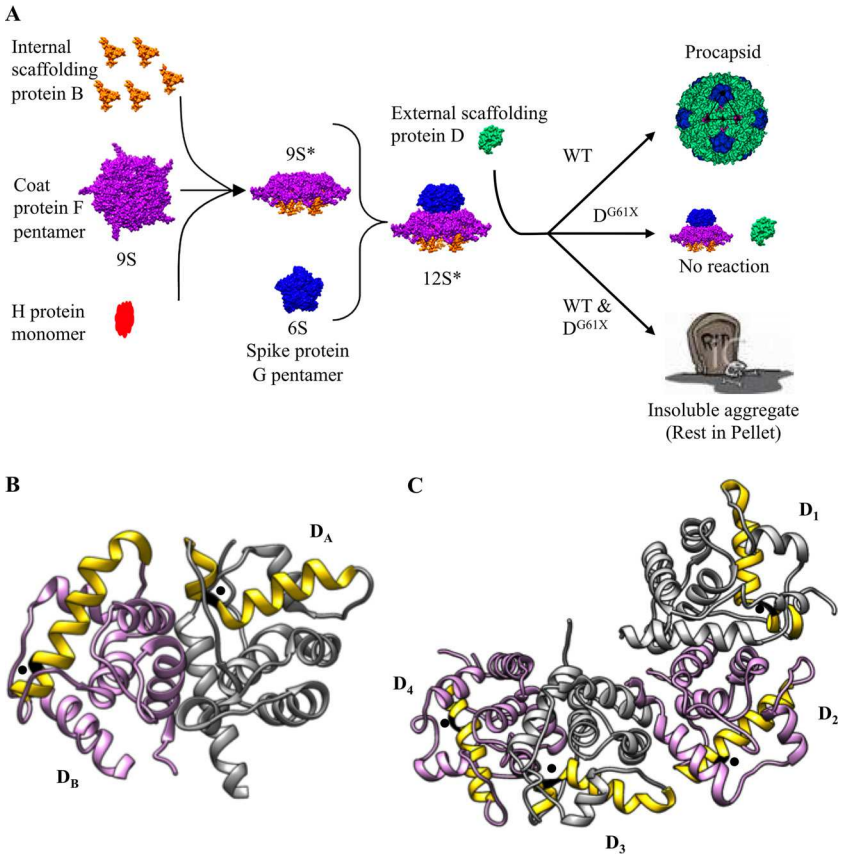

FIG 1 ϕX174 procapsid morphogenesis and X-ray structures of the ϕX174 external scaffolding D protein. (A) The assembly pathway in cells with only wild-type D protein, only D^{G61X} protein (X = valine, aspartic acid, lysine, or proline), and both wild-type and lethal dominant D^{G61X} protein. (B) The assembly-naive D_AD_B dimer (PDB accession number 1TX9 [13]). (C) The D protein tetramer (D_1 to D_4) as arranged in the atomic structure of the procapsid (PDB accession number 1CD3 [14]). Pink depict subunits in which α-helix 3 is straight, whereas this helix is kinked in the gray subunits. α-Helix 3 is highlighted in gold and D^{G61} in black with adjacent black dots to aid visualization.

Proper virion assembly requires a series of precise protein-protein interactions proceeding along an ordered morphogenetic pathway. During the assembly of the T = 1 capsid, early intermediates are directed into large macromolecular structures by transiently associated scaffolding proteins. These proteins mediate conformational switches, lower thermodynamic barriers, and ensure morphogenetic fidelity (9, 10). Unlike most viruses, which use a single scaffolding protein, microviruses utilize a dual-scaffolding-protein system (Fig. 1A), which divides the pathways into two phases. During early assembly, five copies of the internal scaffolding protein B bind the underside of each viral coat protein F pentamer along with one DNA piloting protein H, yielding the 9S* particle (11, 12). These interactions allow the 9S* intermediates to associate with spike protein G pentamers (6S particles) to produce 12S* intermediates. During late assembly, 240 copies of the external scaffolding protein D, most likely arranged as asymmetric dimers, organize 12 12S* particles into procapsids (11, 13). As the procapsid is filled with single-stranded DNA (ssDNA), the internal scaffolding proteins exit the procapsid. Following genome packaging, the external scaffolding proteins dissociate to complete maturation.

The X-ray crystal structure of the ϕX174 assembly-naive external scaffolding protein D is an asymmetric dimer. Each 16,806-Da subunit consists of seven α-helices separated by six loop regions (13). Each dimer subunit assumes a different conformation, D_A and D_B (Fig. 1B). In the procapsid atomic structure (14, 15), each coat protein is decorated with four structurally distinct D proteins, arranged as dimers of dimers, D_1D_2 and D_3D_4

TABLE 1 Fitness values for the wild-type, intermediary, and evolved strains in the presence of each indicated *D* gene expressed in *trans*[a]

Exogenous *D* gene expression	Fitness value (doublings/h, mean ± SD) for the following strain:		
	Wild type	Intermediary[b]	Evolved[c]
None	11.5 ± 0.15	5.7 ± 0.8	5.1 ± 0.5
D^{G61D}	−6.9 ± 0.32	6.2 ± 0.30	11.6 ± 0.21
D^{D34G}	8.9 ± 1.1	6.1 ± 1.0	8.3 ± 0.12

[a]The data presented in this table were adapted from reference 5.
[b]The strain contains three mutations in the viral coat protein F (F^{D44H}, F^{D205N}, and F^{S227P}) and one in the DNA pilot protein H (H^{D136G}).
[c]The strain contains three mutations in the viral coat protein and one in the DNA pilot protein (as for the intermediary strain) and the D^{D34G} mutation in the genome-carried external scaffolding protein *D* gene.

(Fig. 1C). This arrangement allows D protein interactions across the procapsid's 2-fold axes of symmetry. To achieve this unique, non-quasi-equivalent organization, D proteins exist in two major conformations: the D_1 and D_3 subunits are bent 30° in α-helix 3, while the corresponding helices in the D_2 and D_4 proteins are straight (Fig. 1C). This critical kink occurs at glycine residue 61 (D^{G61}) and is also present in the D_A subunit of the assembly-naive dimer (Fig. 1B). Based on Ramachandran plot predictions, only a glycine residue can kink the helix to this extent.

Mutant D genes that encode large side chain substitutions (D^{G61X}, where X is valine, aspartic acid, lysine, or proline) do not complement *nullD* strains and inhibit wild-type (WT) morphogenesis (12). During *nullD* infections, D^{G61X} proteins do not interact with assembly intermediates. However, in wild-type infections (Fig. 1A), these mutant proteins inhibit morphogenesis by removing 12S* intermediates into the insoluble fraction, thus displaying a dominant lethal phenotype (12). As the wild-type D protein forms dimers and higher-order oligomers in solution (11), these observations suggested that lethal dominant G61X proteins cannot self-oligomerize, a hypothesis directly tested in this study.

We previously showed that mutations conferring resistance to the presence of D^{G61X} proteins map to the coat (*F*) and internal scaffolding (*B*) genes. Resistance was not specific to the D^{G61X} mutant allele to which they were selected (5, 6). A strain with a robust resistance phenotype was experimentally evolved. Wild-type ϕX174 was cultured continually by serial passages in exponential-phase cells while the induction of the lethal dominant gene was increased incrementally. The first resistant strain isolated contained three mutations in the coat protein F (F^{D44H}, F^{D205N}, and F^{S227P}), which were identical or similar to resistance mutations isolated in single-step selections. In general, all of these mutations cluster underneath the D_3 subunit in the X-ray structure (12, 16). There was also a mutation in the DNA pilot protein H (H^{D136G}). However, it is unclear whether this mutation contributes to the resistance phenotype. Mutations in this region of the DNA pilot protein are commonly observed during experimental evolution under various selective pressures (17–20). Thus, it may have arisen due to the propagation method. In this study, this strain is referred to as the "intermediary strain." However, the "most evolved" strain achieved optimal fitness after acquiring an additional Asp→Gly mutation within the genome-encoded D protein (D^{D34G}).

In the absence of the D^{G61D} protein, the intermediary and evolved resistant strains demonstrated a decrease in fitness relative to the wild-type virus (Table 1 [data were adapted from reference 5), suggesting that the coat protein mutations may produce prudent less-reactive12S* intermediates that compensate for promiscuous, off-pathway reactions mediated by inhibitory D proteins. The coat protein mutations may allow 12S* particles to entirely exclude mutant dimers from the assembly pathway or from certain locations within the procapsid lattice. Intermediary-strain fitness was not significantly affected by the presence of the D^{G61D} protein (Table 1); however, its presence greatly increased the most evolved strain's fitness (Table 1). The D^{D34G} mutation does not confer a resistance phenotype in an otherwise wild-type background. Thus, the most

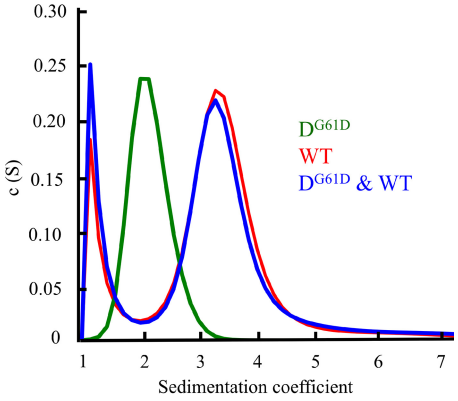

FIG 2 Sedimentation velocity analysis of wild-type D (WT), D^{G61D}, and a mixture of WT and D^{G61D} proteins (1:1).

evolved strain's elevated fitness appeared to be a function of the intragenic D^{D34G} mutation in combination with the other mutations found in the intermediary strain.

Experimental evolution *in vivo* is a powerful tool, providing many genetic insights into possible adaptive mechanisms. However, details needed to test specific mechanistic hypotheses often cannot be determined without more detailed *in vitro* biochemical analyses. In this study, *in vitro* biophysical and biochemical methods were utilized to elucidate the mechanistic details and evolutionary trade-offs of resistance and also determine the extent to which *in vivo* fitness and *in vitro* assembly can be correlated.

RESULTS

The D^{G61D} protein remains monomeric in solution. Earlier results suggested that the inhibitory D^{G61D} protein alone cannot properly dimerize but will form inhibitory oligomers with wild-type subunits (11, 12). To investigate this further, purified mutant and wild-type D proteins (0.5 mg/ml) were examined by analytical ultracentrifugation (AUC). The sedimentation velocity profiles in Fig. 2 indicate that the D^{G61D} and wild-type D proteins sediment at 2.1 S and 3.3 S, respectively. Each single peak was used to estimate the molecular mass for the corresponding sedimenting species. The estimated molecular mass of the D^{G61D} protein was 17.6 kDa, whereas the value obtained for the wild-type D protein was 37.2 kDa. The theoretical molecular masses of a protein D monomer and dimer are 16.8 kDa and 33.6 kDa, respectively. These calculated weights are within 4.6% (monomer) and 9.7% (dimer) of the theoretical values, confirming that D^{G61D} subunits cannot form homodimers.

To determine whether D^{G61D} and wild-type D proteins can form heterodimers, the purified components were mixed at a 1:1 ratio before AUC. This resulted in a single peak consistent with a dimer (Fig. 2), suggesting that homodimeric, wild-type D proteins disassociate and then reassociate with D^{G61D} monomers after mixing. The absence of a monomer peak suggests that once WT/D^{G61D} heterodimers form, they remain stable and do not easily disassociate (see Discussion). Wild-type homodimers and WT/D^{G61D} heterodimers were analyzed by circular dichroism. In agreement with the X-ray structure (13–15), the wild-type D protein homodimer was largely helical. The heterodimers displayed a slight loss of helicity (data not shown). The D^{D34G} protein, which was previously shown to elevate the most evolved strain's fitness, was also analyzed for the ability to form homodimers and heterodimers with the D^{G61D} protein (11, 12). It behaved like the wild-type species in these assays (data not shown). Thus, the D^{D34G} mutation did not appear to alter oligomerization dynamics.

The mutant D^{G61D} protein does not interact with wild-type 12S* early assembly intermediates *in vitro*. During *in vivo* morphogenesis (Fig. 1A), the D^{G61D} protein does not complement a *nullD* strain but inhibits wild-type morphogenesis, thus displaying a dominant lethal phenotype (12). To further characterize this phenomenon, the previously developed *in vitro* assembly system (11) was adapted to analyze assembly

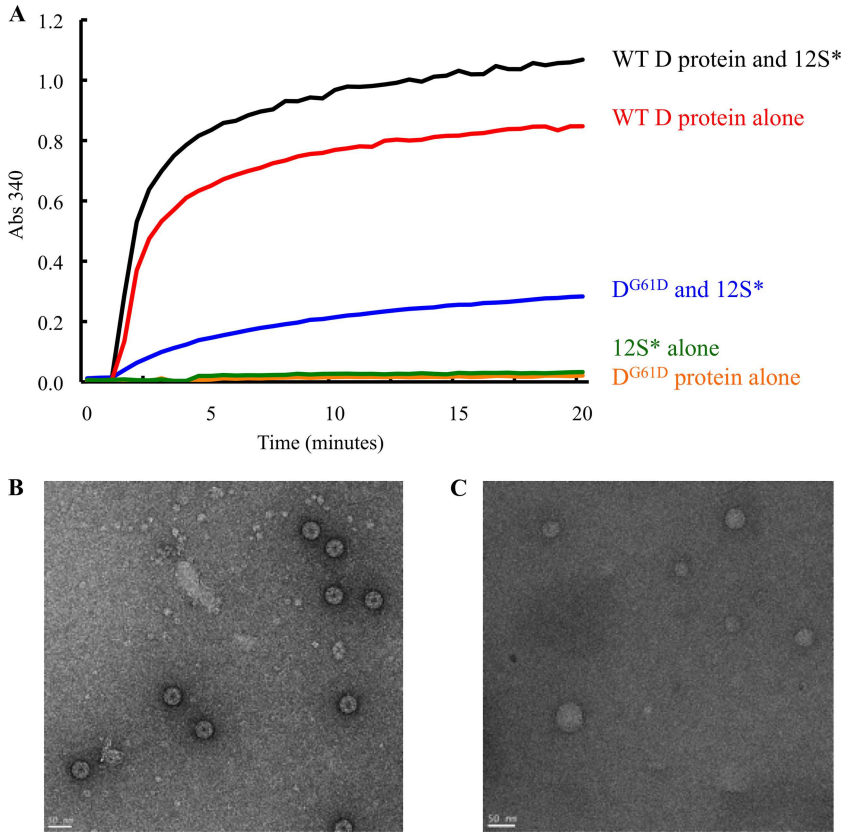

FIG 3 (A) *In vitro* assembly kinetics of purified protein components. The components of each reaction are color coded as indicated in the figure. (B) Electron micrograph of the *in vitro* reaction with WT 12S* plus WT D protein, producing procapsids. (C) Electron micrograph of the WT D protein alone, forming heterogeneous D protein lattice structures lacking internal density.

kinetics. In these experiments, reagents were mixed in the presence of polyethylene glycol, and procapsid assembly was monitored by light scatter at 340 nm as a function of time.

A mixture of wild-type 12S* particles and wild-type D protein produced a rapid increase in detectable light scatter (Fig. 3A), a result consistent with the nucleation and elongation phases of procapsid assembly (21). However, the wild-type D protein alone also produced significant scatter, indicating the formation of larger macromolecular structures. Therefore, samples were examined by electron microscopy. Reaction mixtures containing both wild-type 12S* particles and wild-type D protein produced procapsids with uniform dimensions similar to those of native procapsids (Fig. 3B), whereas the wild-type D protein alone formed a heterogeneous array of protein lattices (Fig. 3C). Similar heterogeneous structures have been reported at wild-type D protein concentrations higher than 4.0 mg/ml (22), conditions likely mimicked by the crowding agent in our assays. Unlike the reactions performed with the wild-type D protein, samples containing only 12S* particles, only the D^{G61D} protein, or a mixture of these two components produced little or no detectable light scatter, indicating the absence of significant macromolecular assembly. Thus, the *in vitro* results are consistent with previous *in vivo* findings.

***In vitro* analysis of assembly kinetics defines the nature of an evolutionary trade-off.** As previously described, serial passages of wild-type ϕX174 in cells expressing the dominant lethal D^{G61D} *D* gene first produced an intermediary strain with a resistant phenotype. That strain contained three substitutions within the viral coat protein F (6). After resistance was established, a mutation in gene *D* arose in the most evolved strain that stimulated fitness (virion doublings per hour) to values as high or

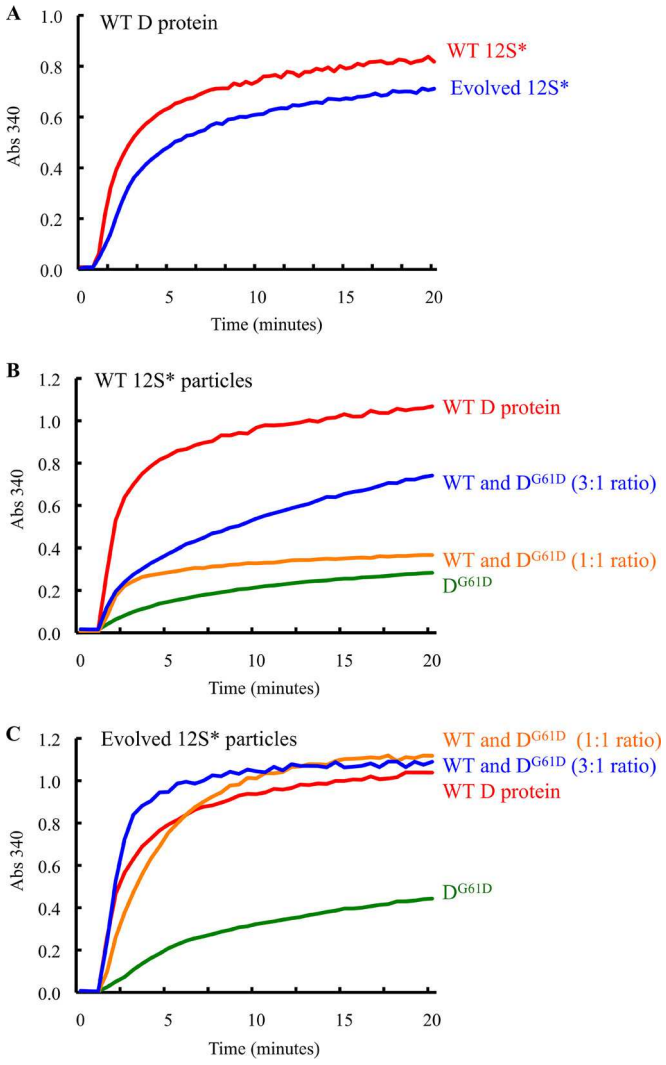

FIG 4 (A) *In vitro* kinetics of procapsid assembly with wild-type or evolved strain 12S* particles. (B) *In vitro* kinetics of procapsid assembly with wild-type 12S* particles supplemented with wild-type D and D^{G61D} proteins. (C) *In vitro* kinetics of procapsid assembly with evolved strain 12S* particles supplemented with wild-type D and D^{G61D} proteins.

higher than that of the uninhibited wild-type strain (Table 1). Although resistant to the inhibitory scaffolding protein, the intermediary strain displayed significantly reduced fitness in the absence of D^{G61D} expression compared to the wild type, indicating that an evolutionary trade-off had occurred (11, 12). To elucidate the nature of the trade-off, the rate of *in vitro* assembly with purified wild-type and evolved-strain 12S* particles in the presence of the wild-type D protein was examined (Fig. 4A). Compared to the wild-type 12S* reaction, the mixture of evolved-strain 12S* particles and wild-type D protein displayed a delayed start and reduced light scattering rate. The delay may indicate that the selection of a resistant coat protein coselected for a less reactive 12S* intermediate in the presence of only wild-type D protein.

***In vitro* analysis of assembly kinetics and liquid chromatography-mass spectrometry distinguishes between two resistance mechanisms.** Two simple contrasting models can explain the resistance mechanism. The coat protein mutations may (i) exclude inhibitory D protein dimers from the assembly pathway or (ii) allow the inhibitory dimers to be productively utilized. To distinguish between these hypotheses, *in vitro* kinetic reactions were carried out with either the wild-type or evolved-strain 12S* particles in the presence of various wild-type and mutant D^{G61D} protein ratios. As

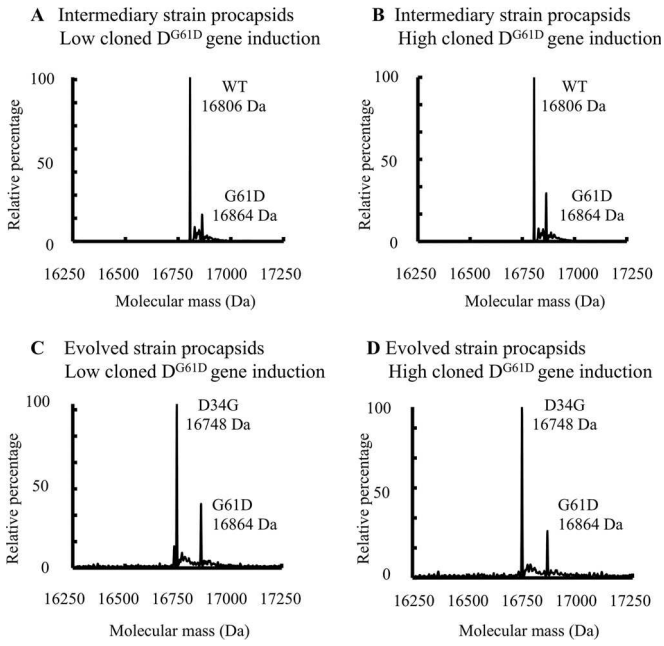

FIG 5 Mass spectrometry verification and calculated masses of the D proteins that were incorporated into *in vivo*-generated procapsids for the intermediary (A and B) and evolved (C and D) strains. During infections, the D^{G61D} cloned gene was induced to produce either low (A and C) or high (B and D) intracellular concentrations of the mutant D protein.

expected, the presence of the D^{G61D} protein lowered procapsid assembly efficiency in the wild-type 12S* reaction (Fig. 4B). Overall, lower WT/D^{G61D} ratios correlated with less efficient assembly reactions. In contrast, the evolved-strain 12S* particles assembled into procapsids more rapidly in the presence of the D^{G61D} protein (Fig. 4C). Moreover, procapsid assembly appeared to be most efficient when the WT and D^{G61D} proteins were present in a 3:1 ratio. The reaction products were examined by electron microscopy, which verified the presence of procapsids (data not shown). The evolved 12S* particle's increase in assembly efficiency in the presence of the D^{G61D} protein favors the model in which the virus evolved to productively utilize the inhibitory protein.

To further verify this conclusion, liquid chromatography-mass spectrometry was used to determine whether the D^{G61D} protein was incorporated into procapsids. Procapsids were generated in lysis-resistant cells infected with the ϕX174 intermediary and evolved strains. The D^{G61D} protein was supplied by a cloned IPTG (isopropyl-β-D-thiogalactopyranoside)-inducible gene. To facilitate isolation and increase yields, an amber mutation was placed in gene *C* to block DNA packaging and the procapsid-to-virion transition. Two different induction conditions were employed: the higher-induction conditions yields a WT/D^{G61D} D protein ratio of approximately 1:1, whereas the lower-induction conditions produce a 3:1 ratio (12).

Figure 5A and B display the calculated masses for the wild-type and D^{G61D} protein peaks of the D proteins found in the procapsids. These values are consistent with their respective theoretical masses: 16,806 (WT) and 16,864 Da (D^{G61D}). There were two D protein peaks found in intermediary-strain procapsids (Fig. 5A and B), demonstrating that both D proteins were incorporated into procapsids generated *in vivo* under low- or high-induction conditions.

D^{D34G} and D^{G61D} together increase the *in vitro* production rate and overall yield of procapsids using the evolved 12S* particle. While the mutations in the viral coat protein contribute to the resistance phenotype, they do not dramatically elevate *in vivo* fitness to uninhibited wild-type levels (5, 6). Instead, the genome-encoded D^{D34G} appears to stimulate fitness, but only in the presence of the dominant lethal D^{G61D} protein and the resistant coat protein mutations. To determine if the D^{D34G} mutation

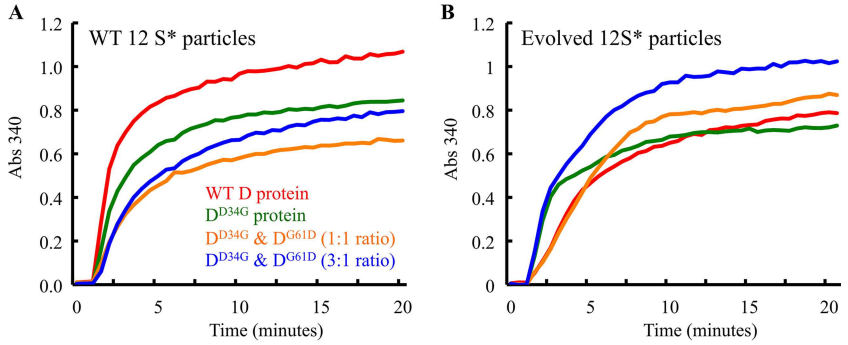

FIG 6 *In vitro* kinetics of procapsid assembly with wild-type, D^{D34G}, and D^{G61D} proteins. (A) WT 12S* particles; (B) Evolved strain 12S* particles. The external scaffolding proteins used in these experiments are color coded as indicated in panel A.

affected assembly kinetics, *in vitro* reactions were conducted with wild-type and resistant 12S* intermediates and various D protein combinations.

Figure 6A shows the light scatter profiles for the *in vitro* assembly reactions over a 20-min period. As expected, the wild-type 12S* reaction mixture supplemented with wild-type D protein produced the highest rate and highest yield of scatter. Reaction mixtures supplemented with the D^{D34G} protein alone or in 1:1 and 3:1 combinations of D^{D34G} to D^{G61D} proteins displayed lower rates of increased light scatter and lower yields. The lowest yield correlated to the highest ratio of D^{D34G} to D^{G61D} D proteins.

In contrast, the resistant 12S* particles exhibited higher yields in assembly reaction mixtures that were supplemented with a combination of the D^{D34G} and D^{G61D} proteins (Fig. 6B). The rate of light scatter was detectably higher when these proteins were present in a respective 3:1 ratio. The wild-type D protein no longer promoted the most efficient reaction as was seen with wild-type 12S* particles (Fig. 6A). These results suggest that the evolved strain adapted a mechanism to utilize the D^{D34G}/D^{G61D} protein heterodimers to increase the efficiency of procapsid assembly. *In vivo* characterization of the evolved strain indicates that optimal fitness was achieved at a relative D^{D34G}-to-D^{G61D} protein ratio of 3:1. The *in vitro* results are in agreement with this observation.

The combination of D^{D34G} with the D^{G61D} proteins has a kinetic effect on assembly. However, it may also increase the amount of D^{G61D} incorporated into evolved-strain procapsids. To investigate this hypothesis, procapsids containing the D^{D34G} and D^{G61D} proteins were generated *in vivo* as described above and examined by liquid chromatography-mass spectrometry. Figure 5C and D represent the results obtained with the evolved-strain procapsids under low and high D^{G61D} gene induction conditions. Based on these spectra, both of the mutant D proteins, D^{D34G} and D^{G61D}, are also incorporated into procapsids, and the calculated masses agree with each protein's theoretical mass (16,748 and 16,864 Da, respectively). However, the relative amount of D^{G61D} protein incorporated into *in vivo*-generated procapsids appears to be independent of the intracellular concentration of the D^{G61D} protein.

The inhibitory D^{G61D} protein appears to be incorporated into procapsids in relatively similar amounts regardless of the presence of the stimulatory D^{D34G} protein. These results indicate that the D^{D34G} protein does not dramatically increase the number of incorporated D^{G61D} proteins and suggest that the stimulatory effects of the D^{D34G} protein are exclusively kinetic.

DISCUSSION

As described in the introduction, lethal dominant ϕX174 external scaffolding D proteins have been characterized, and a resistant strain was experimentally evolved *in vivo* (5, 6, 12, 16). The results indicate that the inhibitory and compensatory mutations target a very specific morphogenetic step: the 12S*-to-procapsid transition. The ability

to reconstitute this reaction *in vitro* (11) allows mechanistic hypotheses to be directly tested and affords the unique opportunity to qualitatively relate *in vivo* fitness to *in vitro* assembly efficiency.

External scaffolding protein oligomerization dynamics and the mechanism of inhibition. As depicted in Fig. 1C, there are four structurally unique D proteins, D_1 to D_4, per coat protein. In subunits D_1 and D_3, a 30° kink in α-helix 3 occurs at glycine residue 61 (G61), whereas this helix is straight in the other two subunits. The X-ray structure predicts that proteins unable to switch between kinked and straight conformations should form long helical oligomers (13), which would not interact with other viral proteins. Although this prediction explains the lack of *in vivo* D^{G61D} protein activity in the absence of the wild-type subunit (12), the results of AUC analysis indicate that the prediction is incorrect. The D^{G61D} protein cannot self-dimerize, a requirement for morphogenesis. The D^{G61D} mutation would inhibit the kinking of α-helix 3. Amino acid residues at the end of the helix participate in dimer formation (13–15). The altered orientation of the helix may inhibit those interactions. The inability to form homodimers is also consistent with the mutant protein's lack of activity in the absence of wild-type subunits.

The D^{G61D} protein did dimerize with the wild-type protein (Fig. 2), which likely allows it to enter the assembly pathway. When mixed at a 1:1 ratio with the wild-type protein, only a single peak was observed after AUC. This suggests that the K_d (dissociation constant) of the wild-type homodimer is greater than the K_d of the heterodimer at equilibrium. If the heterodimers displayed a K_d greater than or equal to that of wild-type dimers, a dimer and monomer peak would have been detected, which was observed when the D^{G61D} protein was in excess (data not shown).

The mechanism of resistance and its inherent evolutionary trade-off. Procapsid assembly of wild-type and evolved strain 12S* particles was analyzed *in vitro* with wild-type D protein. Although procapsids were observed in each sample by electron microscopy, the coat protein resistance mutations created a less reactive 12S* particle. The mutant particles exhibited a lower *in vitro* assembly rate and a decreased yield, which may partially explain the fitness loss in the absence of the inhibitory protein (Table 1).

Assembly was more efficient in the presence of the D^{G61D} protein than in its absence, indicating that the resistant 12S* particles were becoming specialized to assemble with heterodimers. This phenomenon was not previously detected by *in vivo* fitness assays (Table 1). The single-targeted focus of the *in vitro* analysis may have elucidated a detail obscured by more complex and encompassing *in vivo* assays (see below).

Mechanism of stimulation. During experimental evolution, the coat protein mutations conferring resistance appeared first. The last mutation to sweep through the population was D^{D34G} in the genome-carried *D* gene. This single mutation almost doubled fitness in the presence of the D^{G61D} protein (Table 1) and likely specializes assembly with heterodimers. In its absence, fitness was not affected but remained lower than wild type. Resistant 12S* particle assembly kinetics were followed *in vitro* using various combinations of D^{D34G}, D^{G61D}, and wild-type D proteins. Assembly was most efficient and gave the highest yields when reactions mixtures contained a 3:1 D^{D34G}-to-D^{G61D} protein ratio, but it was not possible to attribute this to higher nucleation or elongation rates. Faster nucleation is most reliably detected with a decreased lag phase, which was not observed. The curve's initial slope was steeper right after scatter was detected (data not shown). While this may reflect faster nucleation, faster elongation and higher yields can also affect this region of the graph. The latter may indicate that lower critical concentrations can nucleate assembly, but the presented experiments do not rigorously address this point.

To determine whether the D^{D34G} mutation also increased the amount of D^{G61D} protein allowed into the assembly pathway, procapsids were characterized by liquid chromatography-mass spectrometry. The D^{D34G} mutation did not appear to increase

the amount of D^{G61D} protein found in the procapsid. Thus, the effect of the D^{D34G} mutation appears to be exclusively kinetic. This observation may indicate that the system has evolved an upper limit on the amount of D^{G61D} protein that can be incorporated. Regardless of the induction conditions used to generate procapsids, the amount of incorporated D^{G61D} protein appeared to be constant, approximating one-fourth of the total D protein. This may suggest that the heterodimer is occupying a unique position in the D protein lattice.

Correlating *in vivo* fitness with *in vitro* analyses. In general, *in vitro* assembly efficiency qualitatively correlated with *in vivo* fitness. However, there were some disparities, and the two phenomena could not be quantitatively related. The *in vitro* assay examines a very specific morphogenetic step, whereas *in vivo* fitness measures the entire infection process. *In vitro* assembly reactions begin with substrate levels well above the effective concentrations to nucleate assembly. *In vivo*, the reactants must accumulate to their critical concentrations to nucleate assembly before programmed cell lysis, which occurs independently of progeny formation (23, 24). Several factors could influence when these critical concentrations are achieved in an infected cell. Mutant proteins may require higher critical concentrations and/or be more prone to interact with host cell proteins not present *in vitro*. In either instance, the timing of *in vivo* nucleation could be delayed, which would result in lower fitness. Moreover, procapsids must be filled after formation, which requires the external scaffolding lattice to interact with ssDNA synthesizing and packaging machinery. Inefficient genome synthesis and packaging may account for some disparities. For example, the D^{D34G} mutant in an otherwise wild-type background exhibits fitness values significantly less than wild type (5), yet the protein efficiently assembles procapsids *in vitro* (data not shown).

The redistributed biophysical roles in a two-scaffolding-protein system. The microvirus internal scaffolding protein shares many properties and functions with the scaffolding proteins found in other viruses (7, 9, 10, 14, 15, 25–41). However, it does not physically construct the procapsid or control morphogenetic fidelity. These are functions of the external scaffolding protein. Both *in vitro* and *in vivo*, the external scaffolding protein behaves more like the viral coat protein in other systems, whereas the 12S*-containing coat protein behaves more like a scaffolding protein. For example, coat proteins from other systems form aberrant assemblies in the absence of scaffolding protein, whereas scaffolding proteins alone are relatively inert. When mixed, the scaffolding proteins control fidelity, suppressing the formation of heterogeneous aberrant structures containing only the coat protein (21, 33, 42–50). In contrast, the ϕX174 external scaffolding protein D self-associates to form large heterogeneous spherical complexes (Fig. 2C), whereas coat proteins in the 12S* particles do not self-associate *in vitro*, *in vivo*, or in the assembled procapsid (11, 12, 51). Similarly, the presence of the 12S* particles in reaction mixtures prevents the formation of complexes containing only the external scaffolding coat protein.

MATERIALS AND METHODS

Phage plating, media, buffers, and stock preparation. Media, buffers, plating, and stock preparation have been previously described (52).

***Escherichia coli* cell lines, ϕX174 strains, and plasmids.** The ϕX174 strains and plasmids used in these study have been previously described (5, 6, 11, 12, 53). The *am(C)S10* mutation, which facilitated procapsid isolation, was introduced by site-directed mutagenesis (54). Strains were propagated in BAF7 *supD* (52). The ϕX174 *Δ9D fs440* strain (53) contains a deletion of the first nine *D* gene codons, nucleotides 396 to 419 in the genome sequence, and a frameshift mutation, a deletion of nucleotide 440. It was used to generate wild-type 12S* particles. The *Δ9* mutation was engineered into the evolved ϕX174 strain as previously described (53). the *Δ9D fs440* and *Δ9D* strains were grown in BAF30 pDNco (11). The C900 *E. coli* strain used to generate 12S* particles and procapsids contains the *slyD* mutation, which confers resistance to E protein-mediated lysis (23).

12S* particle and D protein purification. The protocols for 12S* particle and D protein purification have been previously described (11).

AUC and circular dichroism. Sedimentation velocity experiments were performed at 22°C with a D protein concentration of 0.5 mg/ml in 20 mM Tris-HCl, pH 8. The sedimentation at 50,000 rpm in a An-60 Ti rotor was followed by the absorbance at 280 nm over time with a Beckman Optima XL-A analytical ultracentrifuge (AUC) (International Mi-Ss, Inc., Corona, CA). The partial specific volume was calculated by amino acid sequence, and the solvent density was calculated according to the solvent composition using

the Sednterp program found at http://bitcwiki.sr.unh.edu/index.php/Main_Page (55). The sedimentation coefficient distributions were calculated with a continuous c(s) distribution model of Lamm equation solution implemented in the SEDFIT program found at http://www.analyticalultracentrifugation.com/default.htm (56).

Circular dichroism spectra of wild-type and mutant scaffolding proteins were obtained on an AVIV model 62DS spectropolarimeter (Lakewood, NJ) equipped with a single-cell thermoelectric device. Data were collected on 1.0-mg/ml protein solutions at 13°C, from 250 nm to 190 nm in 1.0-nm increments, with a 16-s averaging time per point. The spectrum for baseline correction was identical to the sample solution less protein. Raw data, in millidegrees, were baseline corrected, smoothed, and multiplied by a scaling factor to obtain spectra in units of mean residue ellipticity.

Generation and purification of procapsids synthesized *in vivo*. To isolate *in vivo*-generated procapsids, 1.0 liters of *E. coli* C900 (*slyD*) was grown to a concentration of 1.0×10^8 cell/ml at 37°C. Cells were infected, as described above, with either the intermediary or evolved *am*(*C*)*S10* strain at a multiplicity of infection (MOI) of 3.5. Protein C is essential for DNA packaging. Thus, procapsids accumulate in infected cells (57). Particles were isolated and purified as previously described (58).

Analysis of *in vivo*-generated procapsids by mass spectrometry. *In vivo*-generated procapsids were purified as previously described and were injected onto a Phenomenex Aeris 3.6-μm SB-C_{18} reverse-phase column in 5% acetonitrile and 0.1% formic acid. Species were eluted from the column with a linear gradient from 5% to 95% acetonitrile into a Q-ToF Premier mass spectrometer. Species were identified by mass.

***In vitro* assembly reactions and subsequent analyses.** The 12S* particles and D proteins were mixed with buffer (100 mM Tris-HCl [pH 7.5], 5 mM NaCl, 20 mM $MgCl_2$) at a 1:12 respective molar ratio in 400-μl reaction mixtures at room temperature. The final concentrations of the buffering components were kept constant at 50 mM Tris-HCl, 2.5 mM NaCl, 9.0 mM $MgCl_2$, 20 mM NaCl, and 10% polyethylene glycol (PEG) 3350 as previously described (11). Reactions were followed every 20 s for at least 30 min at a 340-nm wavelength through the use of a Beckman 640 spectrophotometer.

Electron microscopy. The protein samples were diluted into dialysis buffer containing 20 mM Tris-HCl (pH 7.8), 50 mM NaCl, 1 mM $MgSO_4$, 1 mM $CaCl_2$, applied to glow-discharged 400-mesh carbon-only grids (Electron Microscopy Sciences), washed with 2 drops of dialysis buffer, and negatively stained with 1% uranyl acetate. The grids were observed in an FEI Tecnai F20 electron microscope operated at 200 kV and imaged with a Gatan Ultrascan 4000 charge-coupled device (CCD) camera at a magnification of ×65,500 or ×81,200.

ACKNOWLEDGMENTS

This research was supported by National Science Foundation grant MCB 1408217 to B.A.F. and an R.O.A. supplement to J.E.C.

We thank Sarah M. Doore and Aaron P. Roznowski for discussion.

REFERENCES

1. Brown CJ, Millstein J, Williams CJ, Wichman HA. 2013. Selection affects genes involved in replication during long-term evolution in experimental populations of the bacteriophage phiX174. PLoS One 8:e60401. https://doi.org/10.1371/journal.pone.0060401.
2. Doore SM, Fane BA. 2015. The kinetic and thermodynamic aftermath of horizontal gene transfer governs evolutionary recovery. Mol Biol Evol 32:2571–2584. https://doi.org/10.1093/molbev/msv130.
3. Sackman AM, Reed D, Rokyta DR. 2015. Intergenic incompatibilities reduce fitness in hybrids of extremely closely related bacteriophages. PeerJ 3:e1320. https://doi.org/10.7717/peerj.1320.
4. Springman R, Kapadia-Desai DS, Molineux IJ, Bull JJ. 2012. Evolutionary recovery of a recombinant viral genome. G3 (Bethesda) 2:825–830. https://doi.org/10.1534/g3.112.002758.
5. Cherwa JE, Jr, Fane BA. 2011. From resistance to stimulation: the evolution of a virus in the presence of a dominant lethal inhibitory scaffolding protein. J Virol 85:6589–6593. https://doi.org/10.1128/JVI.00261-11.
6. Cherwa JE, Jr, Sanchez-Soria P, Wichman HA, Fane BA. 2009. Viral adaptation to an antiviral protein enhances the fitness level to above that of the uninhibited wild type. J Virol 83:11746–11750. https://doi.org/10.1128/JVI.01297-09.
7. Chen M, Uchiyama A, Fane BA. 2007. Eliminating the requirement of an essential gene product in an already very small virus: scaffolding protein B-free ϕX174, B-free. J Mol Biol 373:308–314. https://doi.org/10.1016/j.jmb.2007.07.064.
8. Rokyta DR, Abdo Z, Wichman HA. 2009. The genetics of adaptation for eight microvirid bacteriophages. J Mol Evol 69:229–239. https://doi.org/10.1007/s00239-009-9267-9.
9. Prevelige PE, Fane BA. 2012. Building the machines: scaffolding protein functions during bacteriophage morphogenesis. Adv Exp Med Biol 726:325–350. https://doi.org/10.1007/978-1-4614-0980-9_14.
10. Zlotnick A, Fane BA. 2010. Mechanisms of icosahedral virus assembly, p 180–202. *In* Agbandje-McKenna M, McKenna R (ed), Structural Virology. Royal Society of Chemistry, London, United Kingdom.
11. Cherwa JE, Jr, Organtini LJ, Ashley RE, Hafenstein SL, Fane BA. 2011. In vitro assembly of the ϕX174 procapsid from external scaffolding protein oligomers and early pentameric assembly intermediates. J Mol Biol 412:387–396. https://doi.org/10.1016/j.jmb.2011.07.070.
12. Cherwa JE, Jr, Uchiyama A, Fane BA. 2008. Scaffolding proteins altered in the ability to perform a conformational switch confer dominant lethal assembly defects. J Virol 82:5774–5780. https://doi.org/10.1128/JVI.02758-07.
13. Morais MC, Fisher M, Kanamaru S, Przybyla L, Burgner J, Fane BA, Rossmann MG. 2004. Conformational switching by the scaffolding protein D directs the assembly of bacteriophage phiX174. Mol Cell 15:991–997. https://doi.org/10.1016/j.molcel.2004.08.023.
14. Dokland T, Bernal RA, Burch A, Pletnev S, Fane BA, Rossmann MG. 1999. The role of scaffolding proteins in the assembly of the small, single-stranded DNA virus phiX174. J Mol Biol 288:595–608. https://doi.org/10.1006/jmbi.1999.2699.
15. Dokland T, McKenna R, Ilag LL, Bowman BR, Incardona NL, Fane BA, Rossmann MG. 1997. Structure of a viral procapsid with molecular scaffolding. Nature 389:308–313. https://doi.org/10.1038/38537.
16. Cherwa JE, Jr, Fane BA. 2009. Complete virion assembly with scaffolding proteins altered in the ability to perform a critical conformational switch. J Virol 83:7391–7396. https://doi.org/10.1128/JVI.00479-09.
17. Bull JJ, Badgett MR, Wichman HA, Huelsenbeck JP, Hillis DM, Gulati A, Ho C, Molineux IJ. 1997. Exceptional convergent evolution in a virus. Genetics 147:1497–1507.
18. Crill WD, Wichman HA, Bull JJ. 2000. Evolutionary reversals during viral adaptation to alternating hosts. Genetics 154:27–37.

19. Wichman HA, Scott LA, Yarber CD, Bull JJ. 2000. Experimental evolution recapitulates natural evolution. Philos Trans R Soc Lond B Biol Sci 355:1677–1684. https://doi.org/10.1098/rstb.2000.0731.
20. Pepin KM, Domsic J, McKenna R. 2008. Genomic evolution in a virus under specific selection for host recognition. Infect Genet Evol 8:825–834. https://doi.org/10.1016/j.meegid.2008.08.008.
21. Prevelige PE, Jr, Thomas D, King J. 1993. Nucleation and growth phases in the polymerization of coat and scaffolding subunits into icosahedral procapsid shells. Biophys J 64:824–835. https://doi.org/10.1016/S0006-3495(93)81443-7.
22. Farber MB. 1976. Purification and properties of bacteriophage phi X 174 gene D product. J Virol 17:1027–1037.
23. Roof WD, Horne SM, Young KD, Young R. 1994. slyD, a host gene required for phi X174 lysis, is related to the FK506-binding protein family of peptidyl-prolyl cis-trans-isomerases. J Biol Chem 269:2902–2910.
24. Zheng Y, Struck DK, Bernhardt TG, Young R. 2008. Genetic analysis of MraY inhibition by the phiX174 protein E. Genetics 180:1459–1466. https://doi.org/10.1534/genetics.108.093443.
25. Fane BA, Prevelige PE, Jr. 2003. Mechanism of scaffolding-assisted viral assembly. Adv Protein Chem 64:259–299. https://doi.org/10.1016/S0065-3233(03)01007-6.
26. Sun Y, Parker MH, Weigele P, Casjens S, Prevelige PE, Jr, Krishna NR. 2000. Structure of the coat protein-binding domain of the scaffolding protein from a double-stranded DNA virus. J Mol Biol 297:1195–1202. https://doi.org/10.1006/jmbi.2000.3620.
27. Tuma R, Parker MH, Weigele P, Sampson L, Sun Y, Krishna NR, Casjens S, Thomas GJ, Jr, Prevelige PE, Jr. 1998. A helical coat protein recognition domain of the bacteriophage P22 scaffolding protein. J Mol Biol 281:81–94. https://doi.org/10.1006/jmbi.1998.1916.
28. Newcomb WW, Trus BL, Cheng N, Steven AC, Sheaffer AK, Tenney DJ, Weller SK, Brown JC. 2000. Isolation of herpes simplex virus procapsids from cells infected with a protease-deficient mutant virus. J Virol 74:1663–1673. https://doi.org/10.1128/JVI.74.4.1663-1673.2000.
29. Thuman-Commike PA, Greene B, Malinski JA, Burbea M, McGough A, Chiu W, Prevelige PE, Jr. 1999. Mechanism of scaffolding-directed virus assembly suggested by comparison of scaffolding-containing and scaffolding-lacking P22 procapsids. Biophys J 76:3267–3277. https://doi.org/10.1016/S0006-3495(99)77479-5.
30. Trus BL, Booy FP, Newcomb WW, Brown JC, Homa FL, Thomsen DR, Steven AC. 1996. The herpes simplex virus procapsid: structure, conformational changes upon maturation, and roles of the triplex proteins VP19c and VP23 in assembly. J Mol Biol 263:447–462. https://doi.org/10.1016/S0022-2836(96)80018-0.
31. Trus BL, Homa FL, Booy FP, Newcomb WW, Thomsen DR, Cheng N, Brown JC, Steven AC. 1995. Herpes simplex virus capsids assembled in insect cells infected with recombinant baculoviruses: structural authenticity and localization of VP26. J Virol 69:7362–7366.
32. Padilla-Meier GP, Gilcrease EB, Weigele PR, Cortines JR, Siegel M, Leavitt JC, Teschke CM, Casjens SR. 2012. Unraveling the role of the C-terminal helix turn helix of the coat-binding domain of bacteriophage P22 scaffolding protein. J Biol Chem 287:33766–33780. https://doi.org/10.1074/jbc.M112.393132.
33. Fu CY, Morais MC, Battisti AJ, Rossmann MG, Prevelige PE, Jr. 2007. Molecular dissection of ø29 scaffolding protein function in an in vitro assembly system. J Mol Biol 366:1161–1173. https://doi.org/10.1016/j.jmb.2006.11.091.
34. Novak CR, Fane BA. 2004. The functions of the N terminus of the phiX174 internal scaffolding protein, a protein encoded in an overlapping reading frame in a two scaffolding protein system. J Mol Biol 335:383–390. https://doi.org/10.1016/j.jmb.2003.09.050.
35. Cortines JR, Motwani T, Vyas AA, Teschke CM. 2014. Highly specific salt bridges govern bacteriophage P22 icosahedral capsid assembly: identification of the site in coat protein responsible for interaction with scaffolding protein. J Virol 88:5287–5297. https://doi.org/10.1128/JVI.00036-14.
36. Newcomb WW, Thomsen DR, Homa FL, Brown JC. 2003. Assembly of the herpes simplex virus capsid: identification of soluble scaffold-portal complexes and their role in formation of portal-containing capsids. J Virol 77:9862–9871. https://doi.org/10.1128/JVI.77.18.9862-9871.2003.
37. Guo PX, Erickson S, Xu W, Olson N, Baker TS, Anderson D. 1991. Regulation of the phage phi 29 prohead shape and size by the portal vertex. Virology 183:366–373. https://doi.org/10.1016/0042-6822(91)90149-6.
38. Mesyanzhinov VV, Sobolev BN, Marusich EI, Prilipov AG, Efimov VP. 1990. A proposed structure of bacteriophage T4 gene product 22—a major prohead scaffolding core protein. J Struct Biol 104:24–31. https://doi.org/10.1016/1047-8477(90)90053-F.
39. Newcomb WW, Homa FL, Brown JC. 2005. Involvement of the portal at an early step in herpes simplex virus capsid assembly. J Virol 79:10540–10546. https://doi.org/10.1128/JVI.79.16.10540-10546.2005.
40. Greene B, King J. 1996. Scaffolding mutants identifying domains required for P22 procapsid assembly and maturation. Virology 225:82–96. https://doi.org/10.1006/viro.1996.0577.
41. Cherwa JE, Jr, Young LN, Fane BA. 2011. Uncoupling the functions of a multifunctional protein: the isolation of a DNA pilot protein mutant that affects particle morphogenesis. Virology 411:9–14. https://doi.org/10.1016/j.virol.2010.12.026.
42. Parker MH, Stafford WF, III, Prevelige PE, Jr. 1997. Bacteriophage P22 scaffolding protein forms oligomers in solution. J Mol Biol 268:655–665. https://doi.org/10.1006/jmbi.1997.0995.
43. Moore SD, Prevelige PE, Jr. 2002. A P22 scaffold protein mutation increases the robustness of head assembly in the presence of excess portal protein. J Virol 76:10245–10255. https://doi.org/10.1128/JVI.76.20.10245-10255.2002.
44. Moore SD, Prevelige PE, Jr. 2002. Bacteriophage p22 portal vertex formation in vivo. J Mol Biol 315:975–994. https://doi.org/10.1006/jmbi.2001.5275.
45. Thuman-Commike PA, Greene B, Malinski JA, King J, Chiu W. 1998. Role of the scaffolding protein in P22 procapsid size determination suggested by T = 4 and T = 7 procapsid structures. Biophys J 74:559–568. https://doi.org/10.1016/S0006-3495(98)77814-2.
46. Newcomb WW, Homa FL, Thomsen DR, Brown JC. 2001. In vitro assembly of the herpes simplex virus procapsid: formation of small procapsids at reduced scaffolding protein concentration. J Struct Biol 133:23–31. https://doi.org/10.1006/jsbi.2001.4329.
47. Kellenberger E. 1990. Form determination of the heads of bacteriophages. Eur J Biochem 190:233–248. https://doi.org/10.1111/j.1432-1033.1990.tb15568.x.
48. Katsura I, Kobayashi H. 1990. Structure and inherent properties of the bacteriophage lambda head shell. VII. Molecular design of the form-determining major capsid protein. J Mol Biol 213:503–511.
49. Earnshaw W, King J. 1978. Structure of phage P22 coat protein aggregates formed in the absence of the scaffolding protein. J Mol Biol 126:721–747. https://doi.org/10.1016/0022-2836(78)90017-7.
50. Prevelige PE, Jr, Thomas D, King J. 1988. Scaffolding protein regulates the polymerization of P22 coat subunits into icosahedral shells in vitro. J Mol Biol 202:743–757. https://doi.org/10.1016/0022-2836(88)90555-4.
51. Bernal RA, Hafenstein S, Olson NH, Bowman VD, Chipman PR, Baker TS, Fane BA, Rossmann MG. 2003. Structural studies of bacteriophage alpha3 assembly. J Mol Biol 325:11–24. https://doi.org/10.1016/S0022-2836(02)01201-9.
52. Fane BA, Hayashi M. 1991. Second-site suppressors of a cold-sensitive prohead accessory protein of bacteriophage phi X174. Genetics 128:663–671.
53. Uchiyama A, Heiman P, Fane BA. 2009. N-terminal deletions of the phiX174 external scaffolding protein affect the timing and fidelity of assembly. Virology 386:303–309. https://doi.org/10.1016/j.virol.2009.01.030.
54. Fane BA, Shien S, Hayashi M. 1993. Second-site suppressors of a cold-sensitive external scaffolding protein of bacteriophage phi X174. Genetics 134:1003–1011.
55. Laue TM, Shah BD, Ridgeway TM, Pelletier SL. 1992. Computer-aided interpretation of analytical sedimentation data for proteins, p 90–125. *In* Harding S, Rowe A (ed), Analytical ultracentrifugation in biochemistry and polymer science. Royal Society of Chemistry, Cambridge, United Kingdom.
56. Schuck P. 2000. Size-distribution analysis of macromolecules by sedimentation velocity ultracentrifugation and lamm equation modeling. Biophys J 78:1606–1619. https://doi.org/10.1016/S0006-3495(00)76713-0.
57. Fujisawa H, Hayashi M. 1977. Functions of gene C and gene D products of bacteriophage phi X 174. J Virol 21:506–515.
58. Uchiyama A, Fane BA. 2005. Identification of an interacting coat-external scaffolding protein domain required for both the initiation of phiX174 procapsid morphogenesis and the completion of DNA packaging. J Virol 79:6751–6756. https://doi.org/10.1128/JVI.79.11.6751-6756.2005.